


 Cite this: *CrystEngComm*, 2018, 20, 4623

Defect evolution in AlN templates on PVD-AlN/sapphire substrates by thermal annealing

 Jianwei Ben,^{ab} Xiaojuan Sun,^{*a} Yuping Jia,^{*a} Ke Jiang,^{ab} Zhiming Shi,^a Henan Liu,^a Yong Wang,^{ab} Cuihong Kai,^{ab} You Wu^{ab} and Dabing Li ^{*a}

AlN is the key material to obtain high performance ultraviolet optoelectronic and microelectronic devices. To obtain high quality AlN, a high temperature annealing method is employed. However, the mechanism of thermal annealing on improving the quality of AlN needs to be further studied. In this work, we focus on the influence of high temperature thermal annealing on the defect evolution in AlN and study the mechanism. AlN epilayers grown by metal-organic chemical vapor deposition (MOCVD) were annealed at different temperatures. The results showed that the full width at half maximum of the (0002) and (10-12) planes for the AlN templates decreased to 147 and 246.8 arcsec after thermal annealing at 1750 °C. Meanwhile many voids appeared in the physical vapor deposition AlN layer. To reveal the mechanism of thermal annealing on improving the quality of AlN, the AlN grown by physical vapor deposition (PVD) was also annealed by high temperature annealing. Atomic force microscopy results showed that realignment and coalescence occurred in the PVD-AlN, which gave the evidence for defect reduction in AlN by the thermal annealing method as well as the existence of AlN voids. The results presented here can not only provide a deeper understanding of the mechanism of the thermal annealing, but also offer a direction to obtain high quality AlN templates.

 Received 11th May 2018,
Accepted 9th July 2018

DOI: 10.1039/c8ce00770e

rsc.li/crystengcomm

Introduction

AlN-based materials have a wide range of applications in the fields of environmental monitoring, biological medicine, national defence security and deep space exploration.^{1,2} The direct band gap of AlN-based materials makes them suitable for fabrication of photoelectric devices such as light-emitting diodes (LEDs), laser diodes (LD) and photodetectors,³⁻⁹ especially for deep ultraviolet (DUV) optoelectronic devices.¹⁰⁻¹² Besides, they are also good candidates for high-power, high-frequency electronic devices.^{13,14} Thus, methods of obtaining high quality AlN have attracted more and more attention.

Many techniques have been employed to decrease the dislocation density and improve the crystal quality of AlN films, such as the interlayer or superlattice method,^{15,16} ammonia (NH₃) pulse-flow growth, migration-enhanced epitaxy (MEE),^{17,18} epitaxial lateral overgrowth (ELO)^{2,19} and so on. Although these methods improve the quality of AlN templates to a certain degree, they have their respective shortcomings.

For example, the interlayer or superlattice method can block dislocation lines from propagating to the surface of AlN, however the growth condition window is narrow and it's easy to lead new dislocation lines into the AlN layer. NH₃ pulse-flow growth, MEE and modified MEE can ameliorate the AlN quality by substantially enhancing Al atom migration, but these methods are limited by low growth rates. ELO is considered to be an effective way to reduce the defect density. However, this method requires *ex situ* patterning, which makes the growth technique more complicated. Recently, thermal annealing has been adopted to further decrease the defects in AlN,^{20,21} which is regarded as a promising way to reduce the defect density in AlN. However, the effect of thermal annealing on decreasing the defects in AlN epilayers needs to be studied further.

Here, we studied the influence of thermal annealing on the defect reduction in AlN. The AlN was grown by MOCVD on a PVD-AlN/sapphire substrate and then annealed at different temperatures. The reasons for the use of PVD-AlN/sapphire as the substrate are as follows: 1) the PVD-AlN is repeatable and uniform,²² which make it suitable to work as the buffer layer between sapphire and AlN grown by MOCVD to obtain a highly uniform AlN epilayer; 2) the PVD-AlN/sapphire substrate is beneficial to the investigation of the effect of thermal annealing on the quality of AlN. The results showed that the defects in the AlN template

^a State Key Laboratory of Luminescence and Applications, Changchun Institute of Optics, Fine Mechanics and Physics, Chinese Academy of Sciences, Changchun 130033, People's Republic of China. E-mail: sunxj@ciomp.ac.cn, ypjia@ciomp.ac.cn, lidb@ciomp.ac.cn

^b University of Chinese Academy of Sciences, Beijing 100039, People's Republic of China

decreased gradually as the thermal annealing temperature increased from 1500 °C to 1700 °C. When the thermal annealing temperature further increased to 1750 °C, the quality of the AlN epilayer was similar to that annealed at 1700 °C. The full width at half maximum (FWHM) of the (0002) and (10-12) planes for the AlN template decreased to 147 and 246.8 arcsec after thermal annealing at 1750 °C. Although there are many research studies on annealing PVD AlN and growing MOCVD AlN on annealed PVD AlN,^{23–25} the defect evolution in AlN has not been studied in detail. To elucidate this, we designed and annealed AlN templates grown by MOCVD on PVD-AlN/sapphire substrates. The growth of crystal grains and the change of stress are observed here, and thus column realignment and coalescence can be strongly proved. The compressive stress formed during the high temperature annealing process will benefit III-nitride epilayer growth, which is another advantage of thermal annealing.

Experimental procedure

PVD-AlN was sputtered on sapphire at 650 °C in a N₂ atmosphere with 4 mTorr. The thickness of PVD-AlN is about 60 nm. For the growth of MOCVD-AlN epilayers (about 600 nm), the precursor gases trimethylaluminum (TMAI) and ammonia (NH₃) were used. The growth temperature was 1277 °C and the pressure was 40 mbar.

The original sample was annealed at 1500 °C, 1600 °C, 1700 °C and 1750 °C for one hour in a N₂ atmosphere. Another sapphire substrate was put on the top of the samples during the thermal annealing process.

A Bruker Multimode-8 AFM was used to confirm the surface morphology. X-ray diffraction rocking curves (XRCs) using a Bruker D8 Discover were adopted to measure the structure properties as well as obtain the dislocation density. Meanwhile, a transmission electron microscope (TEM) was also used to determine the dislocation density. A Raman spectrometer and scanning electron microscope (SEM) were used to measure the residual stress and the cross-section morphology of the AlN templates. Transmission spectra were adopted to determine the optical properties of AlN before and after thermal annealing.

Results and discussion

The quality of the AlN samples was determined by XRC measurement and TEM here. The changes in the XRC FWHM of the (0002) and (10-12) planes after annealing at different temperatures are shown in Fig. 1. Both the FWHM of the (0002) and (10-12) XRCs have an obvious decrease with the increase of annealing temperature. The FWHM of the (0002) and (10-12) planes decreases from 408.6 arcsec to 147 arcsec and 749.5 arcsec to 246.8 arcsec after annealing at 1750 °C, respectively. Since the screw dislocations are mainly caused by the tilt of crystal columns,²⁶ which can border the FWHM of the (0002) XRC,²⁷ the FWHM of the (0002) XRC is usually used to characterize the dislocations with screw components. Similarly, the edge dislocations are caused by the crystal column twist in the plane, which have influence on the FWHM of the (10-12) XRC, so the FWHM of the (10-12) XRC can reflect the density of dislocations with edge components. The decreased FWHM of the (0002) and (10-12) XRCs means that the density of threading dislocations is reduced,²⁸ because the dislocations are mainly caused by the twist and tilt of crystal columns and they emerge from the crystal boundaries.^{29–32} A narrower FWHM of the XRC means that the tilt and twist factors in the AlN crystals have been weakened during high temperature annealing.

According to the relationship between the dislocation density and XRC FWHM:³³

$$\rho_s = \beta_{(0002)}^2 / (2\pi \ln 2 \times |b_c|^2)$$

$$\rho_e = \beta_{(10-12)}^2 / (2\pi \ln 2 \times |b_a|^2)$$

where β is the FWHM of the XRC and $|b_c|$ and $|b_a|$ are the Burgers vector lengths equated to c -axial and a -axial lattice constants. ρ_s and ρ_e stand for the density of dislocations with screw and edge components, respectively. The dislocation densities with screw and edge components of the original sample are calculated to be $3.63 \times 10^8 \text{ cm}^{-2}$ and $3.16 \times 10^9 \text{ cm}^{-2}$, respectively. After thermal annealing at 1700 °C, the densities of dislocations with screw and edge components decrease to $4.81 \times 10^7 \text{ cm}^{-2}$ and $4.47 \times 10^8 \text{ cm}^{-2}$. The FWHM of (0002) nearly unchanged when the annealing temperature increased to 1750 °C, while the FWHM of (10-12) was reduced

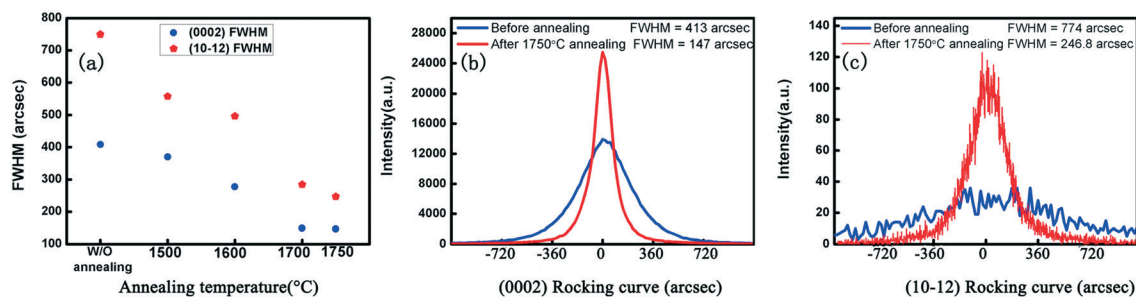


Fig. 1 (a) XRC FWHM of AlN annealed at different temperatures. (b) (0002) and (c) (10-12) XRCs of the AlN template without and with annealing at 1750 °C.

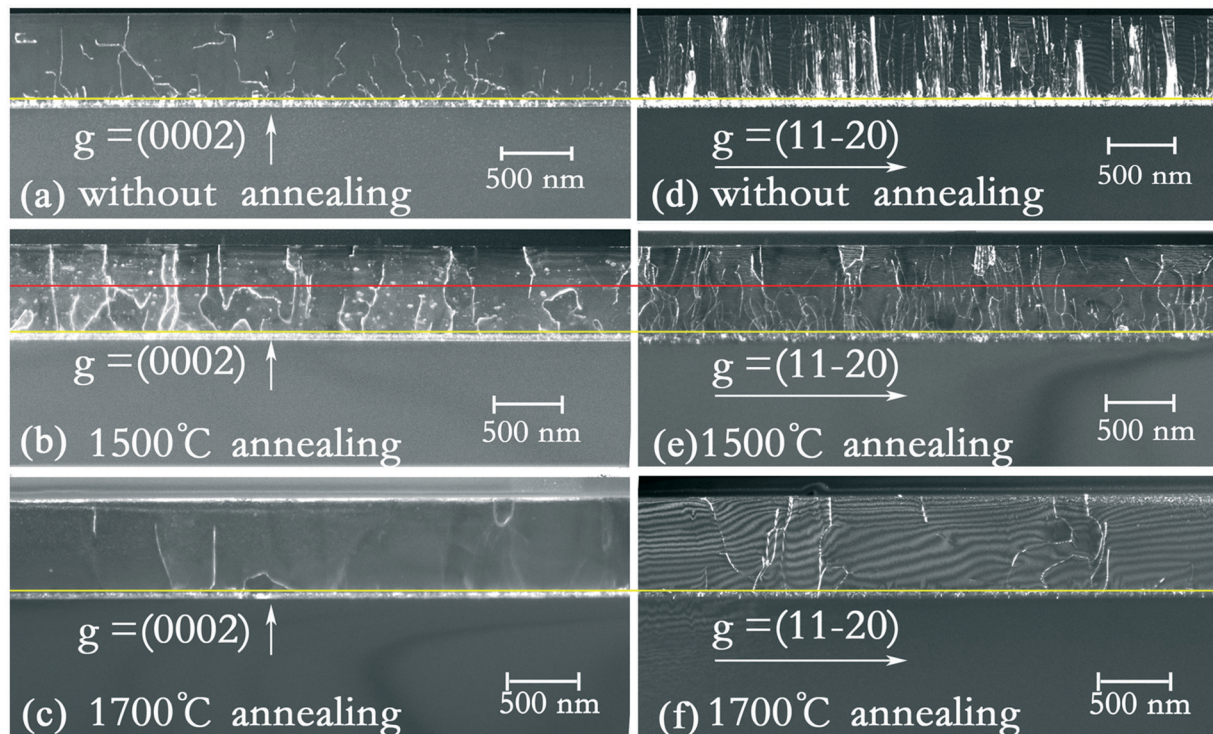


Fig. 2 Dark field TEM observations with $g = (0002)$ for (a) without annealing and with annealing (b) at 1500 °C and (c) at 1700 °C; $g = (11-20)$ for (d) without annealing and with annealing (e) at 1500 °C and (f) at 1700 °C.

a little. It can be concluded that both the screw and edge dislocations have been reduced a lot by the thermal annealing.

The information on dislocations with screw and edge components can be drawn from TEM results with $g = (0002)$ and $g = (11-20)$, respectively. The density of dislocations with screw components decreases from $4.0 \times 10^8 \text{ cm}^{-2}$ to $4.45 \times 10^7 \text{ cm}^{-2}$ after annealing at 1700 °C as shown in Fig. 2(a) and (c). The density of dislocations with edge components decreases from $3.82 \times 10^{10} \text{ cm}^{-2}$ to $3.16 \times 10^8 \text{ cm}^{-2}$, which are calculated from Fig. 2(d) and (f). The TEM results are well consistent with the XRC results, which are shown in Table 1.

The yellow lines in Fig. 2 are the boundaries of MOCVD- and PVD-AlN. Below the yellow line there are many dislocation lines in the PVD-AlN layer because PVD-AlN is polycrystalline with a (0001) preferred orientation. The PVD-AlN layer is much brighter in dark field TEM observation because of its high density dislocations. It can be seen that the dislocation lines for $g = (11-20)$ without annealing are quite straight as shown in Fig. 2(d). As the annealing temperature increases to 1500 °C, the dislocation lines bend and annihilate at almost the same cut-off line, which are shown in Fig. 2(b) and (e).

Table 1 Density of dislocations of the AlN template annealed at 1700 °C

	Density of dislocations with screw components	Density of dislocations with edge components
Calculated via XRC FWHM	$4.81 \times 10^7 \text{ cm}^{-2}$	$4.47 \times 10^8 \text{ cm}^{-2}$
Measured by TEM	$4.45 \times 10^7 \text{ cm}^{-2}$	$3.16 \times 10^8 \text{ cm}^{-2}$

The red line is an obvious dividing line for dislocation bending and annihilation. Many of the dislocation lines bend seriously and annihilate beneath the red line. When the annealing temperature increased to 1700 °C, compared with AlN annealed at 1500 °C, the bend of the edge dislocation lines became more obvious. Besides, the red dividing line (as shown in Fig. 2(e)) disappears in Fig. 2(f), indicating that the annealing temperature is high enough to drive AlN recrystallization with a high degree in all parts. Thus a conclusion can be drawn that high temperature annealing will drive AlN to recrystallize. When the annealing temperature increased to a certain level, the AlN crystal recrystallized completely in all parts and the density of dislocations can be decreased to a large extent.

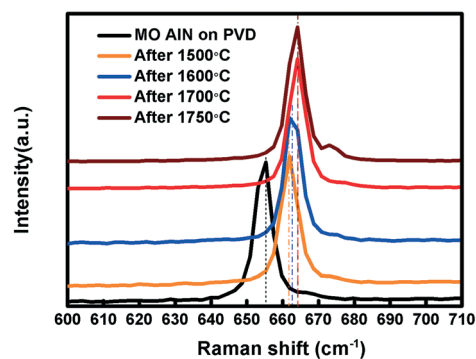


Fig. 3 Raman shift spectra of the AlN templates annealed at different temperatures.

Table 2 Stress state in the AlN layer calculated from the Raman shift spectra

	Without annealing	1500 °C	1600 °C	1700 °C	1750 °C
$E_2(\text{high})$ (cm^{-1})	655.46	661.59	662.56	664.20	664.20
Stress (GPa)	-0.100	1.047	1.231	1.543	1.543

The stress state of the AlN epilayer should be changed when the recrystallization process occurs in AlN. The Raman shift spectra of AlN without and with annealing were taken to confirm the stress state. The $E_2(\text{high})$ mode Raman shift peak of the AlN sample without annealing is at about 655.4 cm^{-1} and blue shifts with high temperature annealing as shown in Fig. 3. Compared with the unstressed AlN Raman peak position sites at around 656 cm^{-1} ,³⁴ the compressive stress in the AlN layer becomes higher. The stress existing in the AlN layer can be calculated by:³⁵

$$\omega = \omega_0 + \omega'P + \omega''P^2$$

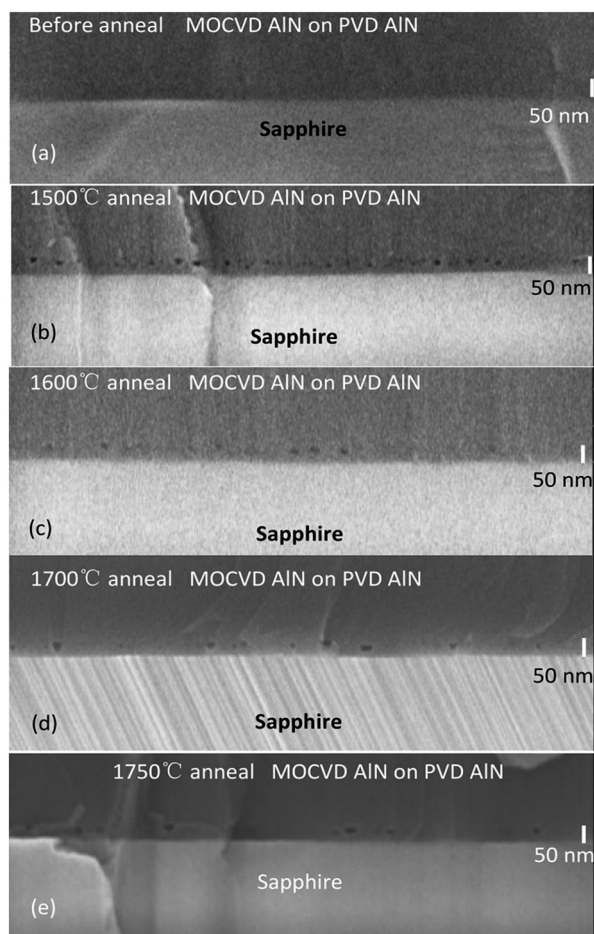
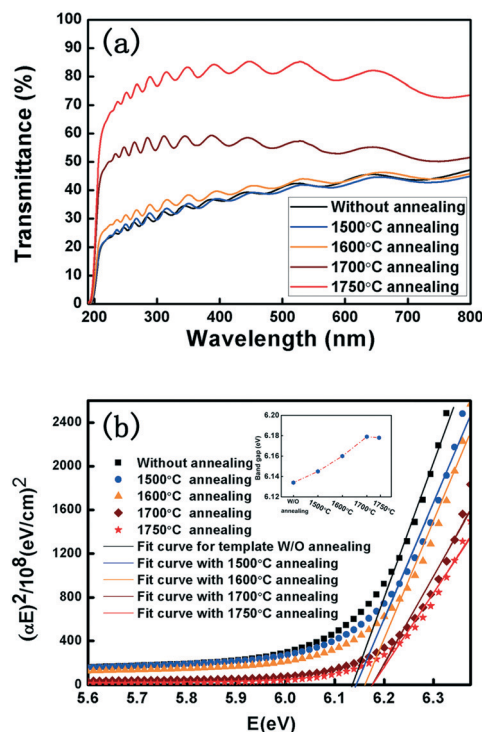
where ω is the phonon frequency of the $E_2(\text{high})$ mode Raman shift obtained from the Raman spectrum and P stands for the

stress existing in the AlN layer. ω_0 , ω' and ω'' are equal to 656 cm^{-1} , $5.39 \text{ cm}^{-1} \text{ GPa}^{-1}$ and $-0.05 \text{ cm}^{-1} \text{ GPa}^{-2}$, respectively. According to the formula, the stress values of AlN are calculated and listed in Table 2. The compressive stress reaches about 1.5 GPa with high temperature annealing above 1700 °C.

The crystal boundaries will reduce the compressive stress resulting from the large mismatch between the AlN and sapphire substrate.^{36,37} When the density of the crystal boundaries decrease, higher AlN crystal quality can be obtained, meanwhile the compressive stress will increase.

SEM measurement was taken to confirm the cross-section morphology change of the AlN template after high temperature annealing. As shown in Fig. 4, it can be found that there are many nanovoids at the interface of PVD-AlN and MOCVD-AlN. According to the crystal column coalescence mechanism we mentioned above, the voids may be formed during the coalescence process of crystal columns.

Furthermore, the effect of thermal annealing on the optical properties of AlN templates is studied. Fig. 5 shows the optical transmission spectra of the AlN templates with and without annealing. Obvious enhancement of transmittance is observed with increasing annealing temperature, exhibiting that the thermal annealing technique is beneficial to the optical properties of the AlN templates. The band edge slopes become sharper with increasing annealing temperature. The slopes are $1.78\% \text{ nm}^{-1}$, $1.80\% \text{ nm}^{-1}$, $2.14\% \text{ nm}^{-1}$, $3.90\% \text{ nm}^{-1}$ and $5.20\% \text{ nm}^{-1}$ for the AlN without annealing and with annealing at 1500 °C, 1600 °C, 1700 °C and 1750 °C, respectively. The

**Fig. 4** (a–e) SEM cross-section images for the information on the interface between PVD-AlN and MOCVD-AlN annealed at different temperatures.**Fig. 5** (a) Optical transmission spectra of the AlN templates annealed at different temperatures, (b) dependence of $(\alpha E)^2$ on (E) , the inset picture shows the band gap of AlN templates annealed at different temperatures.

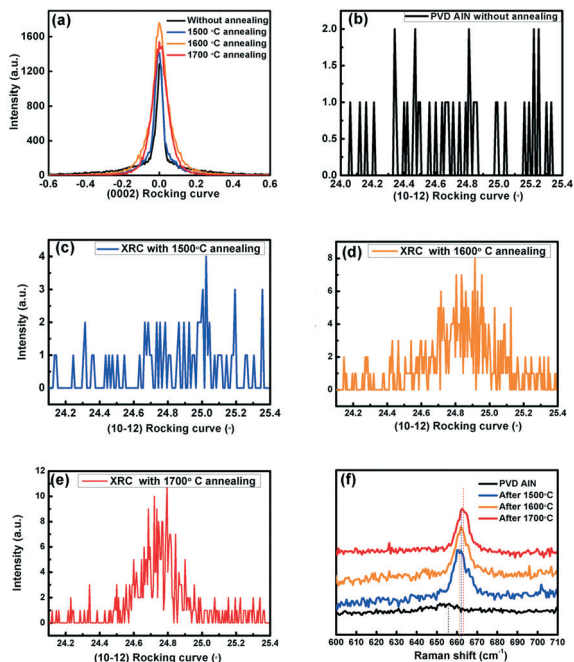


Fig. 6 (a) (0002) XRC of PVD-AlN annealed at different temperatures; (b) (10–12) XRC of PVD-AlN without annealing; (c)–(e) (10–12) XRC of PVD-AlN annealed at 1500 °C, 1600 °C and 1700 °C; (f) Raman spectrum of PVD-AlN annealed at different temperatures.

sharper slopes also prove that the thermal annealing process is also beneficial to the optical quality of AlN.

The relationship of the absorption coefficient α and photon energy E is listed below:

$$\alpha E = A(E - E_g)^{1/2}$$

in which A is the material constant and E_g stands for the band gap of the AlN crystal.

According to the dependence curves of $(\alpha E)^2$ and E , as shown in Fig. 5(b), the band gap increases from 6.134 eV for the AlN template without annealing to around 6.179 eV for that with annealing above 1700 °C. The variation tendency of the band gap is shown in the inset picture of Fig. 5(b). The band gap of AlN increases gradually near to the band gap of bulk AlN (6.2 eV) with the increase of annealing temperature, which means a higher crystal quality of the AlN template is obtained by high temperature annealing.

To reveal the mechanism of thermal annealing on the AlN and the appearance of the voids, as shown in Fig. 4, the PVD-AlN/sapphire substrates were annealed at 1500 °C, 1600 °C and 1700 °C. The PVD-AlN substrate we used in our experiment is polycrystalline with a (0001) preferred orientation, which can be proved by the XRC measurement shown in Fig. 6(a) and (b) and the AFM image in Fig. 7(a).

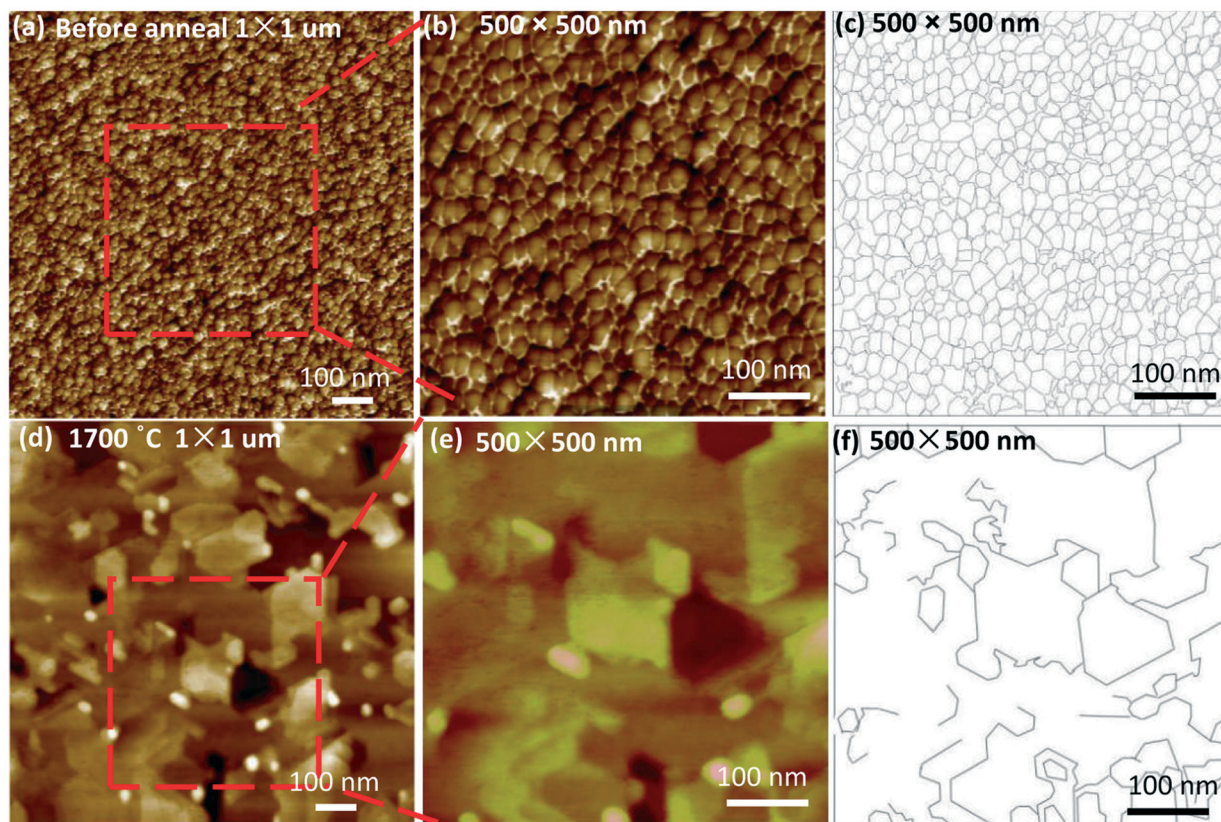


Fig. 7 (a) Surface morphology, (b) enlarged morphology and (c) contour image of PVD-AlN without annealing; (d) surface morphology, (e) enlarged morphology and (f) contour image of PVD-AlN annealed at 1700 °C.

The densities of dislocations and grain boundaries are extremely high in PVD-AlN. From Fig. 6(b), there is no (10–12) rocking curve signal for PVD-AlN without annealing. However, the (10–12) rocking curve becomes visible with the increase of annealing temperature, which means that the polycrystalline AlN converted to single crystal AlN at high temperatures. The same stress evolution tendency appears in the PVD-AlN layer compared with the AlN template, which is characterized by the Raman spectrum shown in Fig. 6(f). The same stress evolution tendency also proves that the recrystallization has occurred in the PVD-AlN layer.

We investigated the surface morphology of PVD-AlN by AFM. The nanostructure in Fig. 7(a) is identified as the crystal grains of PVD-AlN because the size of the nanostructure is pretty small (about 20 nm) and many of them have a hexagonal structure. Here, to demonstrate the crystal grains more clearly, the contour images of the grain boundaries of PVD-AlN without annealing is shown in Fig. 7(c). After annealing at 1700 °C, large grain structures (about 130 nm) appears as shown in Fig. 7(d), which strongly proves that the coalescence of crystal boundaries truly occurs during high temperature annealing.

The contour image of PVD-AlN after annealing at 1700 °C is shown in Fig. 7(f). It can be clearly seen that the bigger and regular structure is formed after annealing compared to the one before annealing. The AFM results are explicit evidence for the recrystallization process of the AlN crystal columns during high temperature annealing. During the annealing process, the realignment and coalescence processes will lead to the merging of small crystal columns into a large one; meanwhile the voids form. The coalescence of the crystal columns in the PVD-AlN layer also gives supporting evidence that the recrystallization process truly takes place during high temperature annealing in AlN materials, which greatly enhances the crystal quality of the AlN materials.

Conclusions

The defects in AlN are reduced by the thermal annealing method and the decreased XRC FWHM of the (10–12) and (0002) planes show drastic reduction of threading dislocations. Based on the FWHM of the XRC, the density of dislocations with screw and edge components of AlN templates is $4.81 \times 10^7 \text{ cm}^{-2}$ and $4.47 \times 10^8 \text{ cm}^{-2}$, respectively. Recrystallization is proved during high temperature annealing and gives the reason for the improvement of the AlN quality. Many voids appear near the interface of MOCVD-AlN and PVD-AlN, which is caused by the coalescence of the high density crystal boundaries in the PVD-AlN layer. The optical performance of the AlN templates is improved after high temperature annealing and the band gap of the AlN epilayer increases from 6.134 eV to around 6.179 eV. The better optical performance makes the AlN template with thermal annealing more suitable to work as the composite substrate for photoelectron devices. This work is beneficial to the understanding of the

improvement mechanism of AlN crystal quality by the thermal annealing method.

Conflicts of interest

There are no conflicts to declare.

Acknowledgements

This work was supported by the National Key R&D Program of China (2017YFB0404104), the National Science Fund for Distinguished Young Scholars (61725403), the National Natural Science Foundation of China (61574142, 61322406, 61704171, 11705206), the Key Program of the International Partnership Program of CAS (181722KYSB20160015), the Special Project for Inter-government Collaboration of the State Key Research and Development Program (2016YFE0118400), the Science and Technology Service Network Initiative of the Chinese Academy of Sciences, the Jilin Provincial Science & Technology Department (20150519001JH, 20180201026GX), the CAS Interdisciplinary Innovation Team, and the Youth Innovation Promotion Association of CAS (2015171).

Notes and references

- X. Sun, D. Li, Y. Chen, H. Song, H. Jiang, Z. Li, G. Miao and Z. Zhang, *CrystEngComm*, 2013, 15, 6066.
- L. Zhang, F. Xu, J. Wang, C. He, W. Guo, M. Wang, B. Sheng, L. Lu, Z. Qin, X. Wang and B. Shen, *Sci. Rep.*, 2016, 6, 35934.
- T. A. Growden, W. Zhang, E. R. Brown, D. F. Storm, D. J. Meyer and P. R. Berger, *Light: Sci. Appl.*, 2018, 7, 17150.
- D. Y. Kim, J. H. Park, J. W. Lee, S. Hwang, S. J. Oh, J. Kim, C. Sone, E. F. Schubert and J. K. Kim, *Light: Sci. Appl.*, 2015, 4, e263.
- J. Li, Z. Liu, Z. Q. Liu, J. Yan, T. Wei, X. Yi and J. Wang, *J. Semicond.*, 2016, 37, 061001.
- Y. Mei, G. Weng, B. Zhang, J. Liu, W. Hofmann, L. Ying, J. Zhang, Z. Li, H. Yang and H. Kuo, *Light: Sci. Appl.*, 2017, 6, e16199.
- D. Zhao, J. Yang, Z. Liu, P. Chen, J. Zhu, D. Jiang, Y. Shi, H. Wang, L. Duan, L. Zhang and H. Yang, *J. Semicond.*, 2017, 38, 051001.
- L. Jiang, J. Liu, A. Tian, Y. Cheng, Z. Li, L. Zhang, S. Zhang, D. Li, M. Ikeda and H. Yang, *J. Semicond.*, 2016, 37, 111001.
- D. Li, X. Sun, H. Song, Z. Li, Y. Chen, H. Jiang and G. Miao, *Adv. Mater.*, 2012, 24, 845.
- D. Li, K. Jiang, X. Sun and C. Guo, *Adv. Opt. Photonics*, 2018, 10, 43.
- D. Dojima, K. Ashida and T. Kaneko, *J. Cryst. Growth*, 2018, 483, 206.
- D. A. Laleyan, S. Zhao, S. Y. Woo, H. N. Tran, H. B. Le, T. Szkopek, H. Guo, G. A. Botton and Z. Mi, *Nano Lett.*, 2017, 17, 3738.
- C. Fu, Z. Lin, P. Cui, Y. Lv, Y. Zhou, G. Dai, C. Luan, H. Liu and A. Cheng, *Appl. Phys. A: Mater. Sci. Process.*, 2018, 124, 299.

- 14 S. Dai, H. Gao, Y. Zhou, Y. Zhong, J. Wang, J. He, R. Zhou, M. Feng, Q. Sun and H. Yang, *J. Phys. D: Appl. Phys.*, 2018, **51**, 035102.
- 15 J. Yan, J. Wang, Y. Zhang, P. Cong, L. Sun, Y. Tian, C. Zhao and J. Li, *J. Cryst. Growth*, 2015, **414**, 254.
- 16 J. Kim, J. Pyeon, M. Jeon and O. Nam, *Jpn. J. Appl. Phys.*, 2015, **54**, 081001.
- 17 H. Hirayama, S. Fujikawa, N. Noguchi, J. Norimatsu, T. Takano, K. Tsubaki and N. Kamata, *Phys. Status Solidi A*, 2009, **206**, 1176.
- 18 R. G. Banal, M. Funato and Y. Kawakami, *Appl. Phys. Lett.*, 2008, **92**, 241905.
- 19 H. Hirayama, S. Fujikawa, J. Norimatsu, T. Takano, K. Tsubaki and N. Kamata, *Phys. Status Solidi C*, 2009, **6**, S356.
- 20 H. Miyake, G. Nishio, S. Suzuki, K. Hiramatsu, H. Fukuyama, J. Kaur and N. Kuwano, *Appl. Phys. Express*, 2016, **9**, 025501.
- 21 H. Fukuyama, H. Miyake, G. Nishio, S. Suzuki and K. Hiramatsu, *Jpn. J. Appl. Phys.*, 2016, **55**, 05FL02.
- 22 L. Chang, Y. Chen and C. Kuo, *IEEE Trans. Electron Devices*, 2014, **61**, 2443.
- 23 H. Miyake, C.-H. Lin, K. Tokoro and K. Hiramatsu, *J. Cryst. Growth*, 2016, **456**, 155.
- 24 J. Hakamata, Y. Kawase, L. Dong, S. Iwayama, M. Iwaya, T. Takeuchi, S. Kamiyama, H. Miyake and I. Akasaki, *Phys. Status Solidi B*, 2018, **255**(5), 1700506.
- 25 C. Huang, P. Wu, K. Chang, Y. Lin, W. Peng, Y. Chang, J. Li, H. Yen, Y. S. Wu, H. Miyake and H. Kuo, *AIP Adv.*, 2017, **7**, 055110.
- 26 M. Nemoz, R. Dagher, S. Matta, A. Michon, P. Vennéguès and J. Brault, *J. Cryst. Growth*, 2017, **461**, 10.
- 27 P. Fini, X. Wu, E. J. Tarsa, Y. Golan, V. Srikant, S. Keller, S. P. Denbaars and J. S. Speck, *Jpn. J. Appl. Phys.*, 1998, **37**, 4460.
- 28 R. G. Banal, M. Imura, D. Tsuya, H. Iwai and Y. Koide, *Phys. Status Solidi A*, 2017, **2**, 214.
- 29 B. Moran, F. Wu, A. Romanov, U. Mishra, S. Denbaars and J. Speck, *J. Cryst. Growth*, 2004, **273**, 38.
- 30 J. Webb, H. Tang, J. Bardwell, S. Moisa, C. Peters and T. MacElwee, *J. Cryst. Growth*, 2001, **230**, 584.
- 31 M. Imura, N. Fujimoto, N. Okada, K. Balakrishnan, M. Iwaya, S. Kamiyama, H. Amano, I. Akasaki, T. Noro, T. Takagi and A. Bandoh, *J. Cryst. Growth*, 2007, **300**, 136.
- 32 F. Ren, Z. Hao, C. Zhang, J. Hu and Y. Luo, *Chin. Phys. Lett.*, 2010, **27**, 068101.
- 33 Y. Chen, H. Song, D. Li, X. Sun, H. Jiang, Z. Li, G. Miao, Z. Zhang and Y. Zhou, *Mater. Lett.*, 2014, **114**, 26.
- 34 A. Dadgara, A. Krosta, J. Christen, B. Bastek, F. Bertram, A. Krtschil, T. Hempel, J. Blasing, U. Haboek and A. Hoffmann, *J. Cryst. Growth*, 2006, **297**, 306.
- 35 M. Kuball, J. M. Hayes, A. D. Prins, N. W. A. van Uden, D. J. Dunstan, Y. Shi and J. H. Edgar, *Appl. Phys. Lett.*, 2001, **78**, 724.
- 36 T. Böttcher, S. Einfeldt, S. Figge, R. Chierchia, H. Heinke, D. Hommel and J. S. Speck, *Appl. Phys. Lett.*, 2001, **78**, 1976.
- 37 A. Claudel, V. Fellmann, I. Gélard, N. Coudurier, D. Sauvage, M. Balaji, E. Blanquet, R. Boichot, G. Beutier, S. Coindeau, A. Pierret, B. Attal-Trétout, S. Luca, A. Crisci, K. Baskar and M. Pons, *Thin Solid Films*, 2014, **573**, 140.